Braz J Phys (2014) 44:308–314
DOI 10.1007/s13538-014-0208-8

CONDENSED MATTER

The Non-Adiabatic Polaron Model Revisited

Fabian E. N. Ramirez · José Antonio Souza

Received: 30 September 2013 / Published online: 15 May 2014

Abstract We revisit Holstein's polaron model to derive an extension of the expression for the thermal dependence of the electrical resistivity in the non-adiabatic small-polaron regime. Our analysis relaxes Holstein's assumption that the vibrational-mode energies $\hbar\omega_k$ are much smaller than the thermal energy $k_B T$ and substitutes a fifth-order expansion in powers of $\hbar\omega_k/k_B T$ for the linear approximation in the expression for the quasiparticle hopping probability in the original treatment. The resulting expression for the electrical resistivity has the form $\rho(T) = \rho_0 T^{3/2} \exp(E_a/k_B T - C/T^3 + D/T^5)$, where C and D are constants related to the molecule–electron interaction energy, or alternatively to the polaron binding energy, and the dispersion relation of the vibrational normal modes. We show that experimental data for the $La_{1-x}Ca_xMnO_3$ ($x = 0.30, 0.34, 0.40$, and 0.45) manganite system, which are poorly fitted by the conventional non-adiabatic model, are remarkably well described by the more accurate expression. Our results suggest that, under conditions favoring high resistivity, the higher-order terms associated with the constants C and D in the above expression should taken into account in comparisons between theoretical and experimental results for the temperature-dependent transport properties of transition-metal oxides.

Keywords Electrical resistivity · Manganites · Transport mechanism · Small polaron

F.E.N. Ramirez · J.A. Souza (✉)
Centro de Ciências Naturais e Humanas, Universidade Federal do ABC, CEP 09090-400, Santo André, SP, Brazil
e-mail: joseantonio.souza@ufabc.edu.br

1 Introduction

The transport properties divide materials into three categories: metallic, insulator, and semiconducting. The electrical conductivity depends primary on the Fermi-level density of states $N(E_F)$. In metals, the Fermi-level density of states is nonzero because one or more bands are partially filled [1, 2]. Conduction depends on electronic states near the Fermi level and is affected by interactions with phonons and impurities. In insulators and semiconductors, on the other hand, the Fermi level lies within a band gap [2], so that $N(E_F) = 0$. Quantum tunneling or thermal excitation across the gap is then necessary to conduct electricity. In insulators, conduction is associated with electronic diffusion [2], and in semiconductors, with thermal activation [3, 4].

Not all metals are good conductors. The states that would be available for conduction can become localized or trapped if, for example, disorder distorts the otherwise periodic lattice potential. The electronic states near E_F can then become localized, even though $N(E_F)$ is nonzero. As in insulators, conduction is still possible via hopping between localized states [5]. Electrical transport is then controlled by the energy splittings separating the localized states and by the hopping distances. In these materials, commonly called Fermi Glasses [5], two electrical transport processes become possible: (1) if the states are strongly localized, the overlap between wavefunctions decreases rapidly with distance, and electrons can only transition to the nearest states, i. e., they can only undergo nearest-neighbor hopping; (2) if the states are more weakly localized, and the thermal energy is insufficient to allow charge transfer to the closest states, hopping between randomly positioned states can be energetically favorable. In this variable-range hopping scenario, the electron exchanges energy with a phonon while hopping between the two overlapping localized states. This

will only be possible if the Fermi-level density of states $N(E_F)$ is nonzero, a condition satisfied by weak Anderson localization [5].

In several doped transition-metal oxides, optical measurements reveal a gap [6–8], within which the density of states vanishes, so that $N(E_F) = 0$. In manganese doped oxides, in particular, the electrical resistivity has been shown to follow the variable-range hopping model; at low temperatures, however, the gap closes and $N(E_F)$ becomes finite. Doped transition metal oxides, by contrast, have been recognized to show strongly correlated physical properties, due to interplay between lattice, spin, charge, and orbital degrees of freedom [9].

The interplay between lattice distortion and charge transport gives rise to a number of effects. The interaction between the electron charge and lattice-atom dynamics, first studied by Holstein [10], gives rise to a quasiparticle called the polaron. In Holstein's polaronic model an electron travels slowly along a one-dimensional molecular crystal constituted by N diatomic molecules. The n-th molecule has a single vibrational degree of freedom, represented by the deviation from equilibrium x_n of the internuclear separation. The system Hamiltonian is the sum of three terms, $H_S = H_e + H_L + H_{int}$. The electronic contribution H_e consists of the electronic kinetic energy and effective one-electron periodic potential. The lattice Hamiltonian H_L accounts for the kinetic and potential energies of the lattice particles. Finally, H_{int} describes the local interaction between the electron and the molecules.

If the electron-molecule interaction is sufficiently strong, the lattice atoms are displaced to new equilibrium positions and define a potential well for the electrons. A polaron is formed when the electron occupies a bound state of this potential well. The motion of the electron will then be dressed by the induced lattice-deformation. If the size of the deformation is comparable to the lattice spacing a, the quasiparticle is called a small polaron. In this model, the energy of the molecule-electron local interaction grows linearly with the deviation x_n: $E(x_n) = -Ax_n$ [10]. Holstein used the tight-binding approach to describe electronic motion in the molecular crystal and wrote the electronic wave function $\Psi(\mathbf{r}, x_n)$ as a superposition of local molecular functions $\Phi(\mathbf{r} - n\mathbf{a}, x_n)$ [11].

The time-dependent Schrodinger equation $i\hbar\partial\Psi/\partial t = H_S\Psi$ then yields a non-vanishing electronic-overlap J [11], which is related to the polaron binding energy by the equality $E_p = -2J + A^2/(2M\omega_0)^2$, where M is the reduced mass and ω_0 is the optical-phonon frequency. E_p is the energy needed to dissociate the small polaron, i. e., to create a free electronic state in a band whose width W_B is determined by the overlap integral: $W_B = 2J$. At high temperatures, $T > \Theta_D/2$, the overlap J allows electronic hopping via off-diagonal transitions [11]. In such transitions, a few vibrational quantum numbers N_k change by one or two when the electron hops to a neighboring site, so that the initial and final states have different vibrational energies, and transport must be thermally activated, the electronic motion consisting of random hops between neighboring sites. The electrical conductivity σ is then proportional to the thermally averaged probability W_T of an electron jumping to a neighboring site [11, 12],

$$\sigma = \frac{ne^2a^2W_T}{k_BT}, \tag{1}$$

where a is the hopping distance, k_B is the Boltzmann constant, and n is the carrier density.

The probability W_T takes different forms and values depending on the physical regime. In the *adiabatic regime*, an electron can hop more than once to the neighboring sites in the period of the relevant optical vibration. In other words, the hopping frequency Ω_0, i. e., the average frequency of hop attempts to neighboring sites, is larger than the optical phonon frequency ω_0. The hopping probability for the polaron is then high, and the electrical resistivity $\rho \equiv 1/\sigma$ is given by the expression

$$\rho(T) = \rho_0 T \exp(E_a/k_BT). \tag{2}$$

Here, E_a is the activation energy, and the prefactor is given by the expression $\rho_0 = 2\pi k_B/g_d n a^2 e^2 \omega_0$, where g_d is a hopping-geometry factor [13].

In the *non-adiabatic regime*, the hopping frequency is smaller than the optical-phonon frequency, $\Omega_0 < \omega_0$, and the hopping probability for the polaron is small. This regime is activated when the overlap integral constant J is very small. Conventional time-dependent perturbation theory then yields the following expression for the hopping probability W_T [11]:

$$W_T = \frac{J^2}{\hbar^2}\left(\frac{2\pi}{\frac{1}{\pi}\int_0^\pi 2\gamma_k {\omega_k}^2 \operatorname{csch}\left(\frac{\hbar\omega_k}{2k_BT}\right) \mathrm{d}k}\right)^{\frac{1}{2}} \times \exp\left(\frac{-1}{\pi}\int_0^\pi 2\gamma_k \tanh\left[\frac{\hbar\omega_k}{4k_BT}\right] \mathrm{d}k\right), \tag{3}$$

where

$$\gamma_k = A^2\frac{1-\cos k}{2M{\omega_k}^3\hbar}, \tag{4}$$

and

$${\omega_k}^2 = {\omega_0}^2 + {\omega_1}^2\cos k. \tag{5}$$

The frequency ω_1 depends on the coupling between the local vibrational modes and the normal-mode wavenumber $k = 2\pi\ell/N$, where N is the number of molecular sites, and ℓ is an integer.

Equation (3) can be analytically solved in the classical limit $\hbar\omega_k/k_BT << 1$. The hyperbolic cosecant is then approximately equal to the inverse of its argument, $\mathrm{csch}(\hbar\omega_k/k_BT) \approx k_BT/\hbar\omega_k$, while the hyperbolic tangent is approximately equal to its argument, $\tanh(\hbar\omega_k/k_BT) = \hbar\omega_k/k_BT$. With these approximations, the hopping probability can be computed analytically, and the electrical resistivity is given by the equality

$$\rho(T) = \rho_0 T^{3/2} \exp(E_a/k_BT), \tag{6}$$

with a prefactor ρ_0 that is related to the hopping frequency Ω_0 by the following equation [14]:

$$\rho_0 = \frac{k_B}{na^2e^2\Omega_0 T^{1/2}} \tag{7}$$

Equations (2) and (6) have been used to interpret electrical resistivity data from numerous systems, including manganites[13, 15–18]. In many compounds, however, neither the adiabatic (2) nor the non-adiabatic (6) polaronic model are adequate to describe electrical transport [18–24]. In such cases, one usually looks for other mechanisms to derive expressions that fit the experimental data better. In certain cases, the polaron model was discarded in favor of alternative mechanisms and entirely different physics because small deviations separated the theoretical predictions from experimental results.

In order to better understand these deviations, we have gone back to Holstein's derivation of the non-adiabatic polaron model. Since the hopping probability is especially sensitive to changes in the argument of the exponential on the right-hand side of (3), first-order truncation of the series expansion for the hyperbolic tangent in the integrand is only justified for very small $\hbar\omega_k/k_BT$. For larger ratios, additional terms must be included. We have, therefore, kept the first-, third-, and fifth-order contributions to the series, with the following result:

$$\tanh\left(\frac{\hbar\omega_k}{4k_BT}\right) \approx \frac{\hbar\omega_k}{4k_BT} - \frac{1}{3}\left(\frac{\hbar\omega_k}{4k_BT}\right)^3 + \frac{2}{15}\left(\frac{\hbar\omega_k}{4k_BT}\right)^5 \tag{8}$$

Substitution of (8) into (3) leads to an integrable expression for the argument of the exponential in the right-hand side. The integral in the denominator of the first factor on the right-hand side can be computed to first order in $\hbar\omega_k/k_BT$. To this end, we substitute the inverse of the argument for the hyperbolic cosecant in the integrand, which leads to the expression:

$$\begin{aligned} I_1 &\equiv \frac{1}{\pi}\int_0^\pi 2\gamma_k {\omega_k}^2 \,\mathrm{csch}\left[\frac{\hbar\omega_k}{2k_BT}\right] \mathrm{d}k \\ &\approx \frac{4k_BT}{\hbar\pi}\int_0^\pi \gamma_k\omega_k \,\mathrm{d}k, \end{aligned} \tag{9}$$

which we rewrite in the form

$$I_1 = \frac{8E_ak_BT}{\hbar^2}, \tag{10}$$

with the activation energy E_a defined by the equality [11]

$$\begin{aligned} E_a &= \frac{1}{\pi}\int_0^\pi \frac{\gamma_k\hbar\omega_k}{2}\,\mathrm{d}k \\ &= \frac{1}{\pi}\int_0^\pi (A^2/4M{\omega_k}^2)(1-\cos k)\,\mathrm{d}k \end{aligned} \tag{11}$$

With the right-hand side of (8) substituted for the hyperbolic tangent, the integral within the argument of the exponential function on the right-hand side of (3) can be written in the form:

$$\begin{aligned} I_2 =& \frac{-2}{\pi}\int_0^\pi \gamma_k\left(\frac{\hbar\omega_k}{4k_BT}\right)\mathrm{d}k + \frac{2}{3\pi}\int_0^\pi \gamma_k\left(\frac{\hbar\omega_k}{4k_BT}\right)^3\mathrm{d}k \\ &- \frac{4}{15\pi}\int_0^\pi \gamma_k\left(\frac{\hbar\omega_k}{4k_BT}\right)^5\mathrm{d}k \end{aligned} \tag{12}$$

Given the definition (11) of the activation energy, we can rewrite 12 in the form:

$$\begin{aligned} I_2 =& -\frac{E_a}{k_BT} + \frac{2}{3\pi}\int_0^\pi \gamma_k\left(\frac{\hbar\omega_k}{4k_BT}\right)^3\mathrm{d}k \\ &- \frac{4}{15\pi}\int_0^\pi \gamma_k\left(\frac{\hbar\omega_k}{4k_BT}\right)^5\mathrm{d}k \end{aligned} \tag{13}$$

We can now substitute (4) and (5) for γ_k and ω_k^2, respectively, on the right-hand side of (13) to obtain the expression:

$$\begin{aligned} I_2 &= -\frac{E_a}{k_BT} + \frac{\hbar^2A^2}{192M\pi{k_B}^3T^3}\int_0^\pi (1-cosk)\,\mathrm{d}k \\ &- \frac{2\hbar^4A^2}{15360M\pi{k_B}^5T^5}\int_0^\pi {\omega_k}^2(1-cosk)\,\mathrm{d}k \\ &= -\frac{E_a}{k_BT} + \frac{\hbar^2A^2}{192M{k_B}^3T^3} \\ &- \frac{\hbar^4A^2}{15360M{k_B}^5T^5}(2{\omega_0}^2 - {\omega_1}^2) \end{aligned} \tag{14}$$

We then substitute (11) and (14) for the integrals in (3) to obtain a closed expression for the hopping probability:

$$W_T = \frac{J^2}{\hbar^2}\left[\frac{2\pi\hbar^2}{8E_ak_BT}\right]^{1/2}\exp\left[\frac{-E_a}{k_BT} + \frac{C}{T^3} - \frac{D}{T^5}\right] \tag{15}$$

where the parameters C and D are given by the expressions

$$C = \frac{A^2\hbar^2}{192M{k_B}^3}, \tag{16}$$

and

$$D = \frac{A^2\hbar^4}{15360Mk_B{}^5}(2\omega_0{}^2 - \omega_1{}^2), \tag{17}$$

and we recall that A is the constant in Holstein's expression for the deformation energy $E(x_n) = -Ax_n$, which determines the polaron binding energy $E_p = -2J + (A^2/2M\omega_0{}^2)$ and the activation energy in (11).

Equation (15) yields the following generalization of (6):

$$\rho(T) = \rho_0 T^{3/2} \exp\left(\frac{E_a}{k_B T} - \frac{C}{T^3} + \frac{D}{T^5}\right). \tag{18}$$

The prefactor ρ_0 on the right-hand side of (18) is still expressed by (7), with a temperature-dependent hopping frequency expressed by the equality

$$\Omega_0 = \frac{k_\beta T}{na^2e^2\rho(T)} \exp\left(\frac{E_a}{k_B T} - \frac{C}{T^3} + \frac{D}{T^5}\right) \tag{19}$$

Equations (16) and (17) show that the two extra terms C/T^3 and D/T^5 on the right-hand sides of (18) and (19) are proportional to A^2. The corrections C/T^3 and D/T^5 may become important when the deformation energy $E(x_n)$ and, consequently, the polaron binding and activation energies E_p and E_a increase sharply due to, for example, doping or disorder, which tend to raise the high electrical resistivity. The term fifth-order D/T^5 also tends to grow in proportion to the squares of the optical frequency ω_0 and dispersion coefficient ω_1.

2 Results and discussion

Equation (18) is a refined version of (6), more accurate because terms up to fifth-order have been kept in the expansion of the hyperbolic tangent in the argument of the exponential on the right-hand of (3). To highlight the significance of the improvement, we now compare our expression for the temperature-dependent resistivity in the non-adiabatic regime with experimental results. More specifically, we fit electrical resistivity data for $La_{1-x}Ca_xMnO_3$ (x = 0.30, 0.34, 0.40, and 0.45) with (18).

The sample preparation and electrical resistivity measurements have been described in detail elsewhere [25]. The family under study undergoes a structural phase transition from rhombohedral ($R\bar{3}c$) to orthorhombic ($Pnma$) at the high temperatures $T_{RO} = 715$ and 800 K, for $x = 0.30$ and 0.45, respectively. The room temperature electrical resistivities are $\rho = 0.013$, 0.0095, 1.1, and 18 Ωcm for $x = 0.30$, 0.34, 0.40, and 0.45, respectively. The resistivity is therefore minimum for $x = 0.34$ and rises rapidly for higher concentrations. At low doping ($x = 0.30$ and 0.34), the non-adiabatic regime expression (6) proves reliable in the $Pnma$ phase, below $T_{RO} \sim 715$ K, while the adiabatic regime is activated above T_{RO}, in the $R\bar{3}c$ phase [26].

At higher doping levels, $x = 0.40$ and 0.45, however, we have found that neither the mathematical expression describing the temperature-dependent resistivity of the small polaron model in the non-adiabatic regime nor the expression describing the resistivity in the adiabatic regime fit the experimental data. In view of the discrepancies, we have revisited the non-adiabatic regime and turned to (18) to interpret the experimental results. For completeness and comparison, we have fitted the data for all samples, ($x = 0.30$, 0.34, 0.40, and 0.45) with both the conventional equality (6) and the more accurate expression (18).

Figure 1 shows the thermal dependence of the electrical resistivity, fitted by (18), for $x = 0.30$ and 0.34. The insets show fits with (6). Both equations describe very well the electrical resistivities of the two samples. The polaron activation energies E_a extracted from the fits with (6) are 132(5) meV and 100(5) meV for $x = 0.30$ and 0.34, respectively. The fits with (18) yield the activation energies $E_a = 128(4)$ meV and 111(4) meV for $x = 0.30$ and 0.34, respectively. The excellent fits and the nearly equal activation energies indicate that the linear approximation $\tanh(\hbar\omega_k/4k_BT) \approx \hbar\omega_k/(4k_BT)$ is adequate for the low-resistivity samples.

Figure 2 shows analogous fits for $x = 0.40$ and 0.45. As in Fig. 1, the main plots show that (18) displays excellent fits of the temperature-dependent resistivity. By contrast, the red solid lines representing (6) in the insets fail to describe

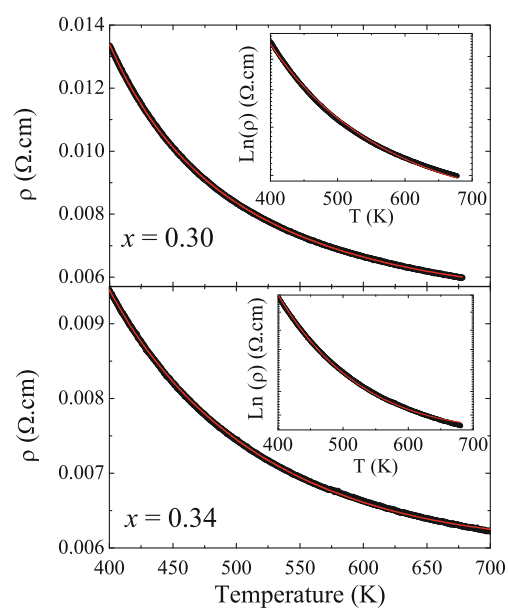

Fig. 1 (*Colored online*) Electrical resistivity as a function of temperature for $x = 0.30$ and 0.34. The *red solid lines* in the main plots represent fits with (18), while the *insets* show fits with (6)

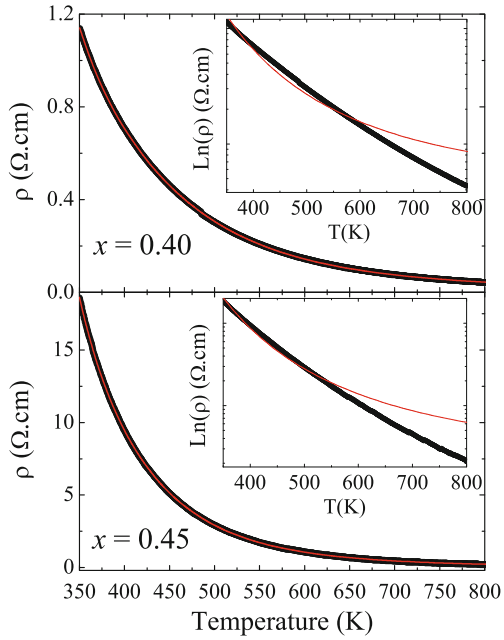

Fig. 2 (*Colored online*) Electrical resistivity as a function of temperature for $x = 0.40$ and 0.45. The *solid red lines* represent fits to the data using the (18). The *insets* show fits of (6) to the same data

$\rho(T)$.[1] These results indicate that the high-resistivity samples satisfy poorly the condition $\hbar\omega_k \ll 4k_BT$, so that the higher-order terms cannot be neglected in the expansion of the hyperbolic tangent, and call for discussion of the influence of the cubic and fifth-order terms.

The temperature dependencies of C/T^3 and D/T^5 for the four studied concentrations are displayed in Fig. 3. Both terms C/T^3 and D/T^5 are much larger for $x = 0.40$ and 0.45 than for the lower concentrations and both decay rapidly with temperature. We see that the two corrections to the conventional treatment are only important in the high-resistivity regime, at sufficiently low temperatures and high concentrations. In the temperature range in our study, the $x = 0.30$ and 0.34 samples always lie outside that regime and are therefore well described by the linear-expansion leading to (6). To check that terms of order above five need not be taken into account, we have carried out a similar analysis including the seventh-order term. The resulting correction being very small, we conclude that our fifth-order expansion is sufficiently accurate.

Figure 4 shows the activation energy E_a, deformation coefficient A, and fifth-order coefficient D resulting from the fittings. All three parameters rise sharply as the concentration grows above $x = 0.35$. Larger A's imply larger electron-molecule local-interaction energies and polaron binding energies. The enhanced activation energies at larger concentrations point to more localized charge carriers, i. e., to larger electrical resistivities.

The fitting parameters also give access to the frequencies ω_0 and ω_1 that define the vibrational frequencies ω_k. We only have to assume that $\omega_1 < \omega_0$ to evaluate the integral on the right-hand side of (11) and obtain the following result:

$$E_a = \frac{A^2}{2M}\left(\frac{1}{{\omega_0}^2 - {\omega_1}^2 + \sqrt{{\omega_0}^4 - {\omega_1}^4}}\right). \tag{20}$$

We can now invert the system of (16), (17), and (20) to determine ω_0 and ω_1 as functions of the fitting parameters E_a, C, and D. The result is the following quartic equation:

$$4{\omega_0}^4 + b{\omega_0}^2 + c = 0. \tag{21}$$

where $b = 2N - 4L$ and $c = L^2 + N^2$, with the shorthands $L \equiv (80{k_B}^2/\hbar^2)(D/C)$ and $N \equiv (96{k_B}^3/\hbar^2)(C/E_a) - L$.

Once (21) is solved for ω_0, the frequency ω_1 can be obtained from the equality

$$\omega_1^2 = 2{\omega_0}^2 - L. \tag{22}$$

The four solutions of (21) have the forms:

$$\omega_0 = \pm\frac{\sqrt{2}}{4}\sqrt{-b + \sqrt{b^2 - 16c}} \tag{23}$$

and

$$\omega_0 = \pm\frac{\sqrt{2}}{4}\sqrt{-b - \sqrt{b^2 - 16c}} \tag{24}$$

Given E_a, C, and D, it is a simple matter to compute the right-hand sides of (23) and (24). Out of the four solutions, only one yields real positive frequencies ω_0 and ω_1. For $x = 0.30$, 0.34, 0.4, and 0.45, we find $\nu_0 = \omega_0/2\pi = 9.177 \times 10^{13}$ Hz, 3.538×10^{13} Hz, 4.985×10^{13} Hz and 4.859×10^{13} Hz, and $\nu_1 = \omega_1/2\pi = 9.175 \times 10^{13}$ Hz, 3.438×10^{13} Hz, 4.772×10^{13} and 4.668×10^{13} Hz, respectively. For all concentrations, ω_1 is close to ω_0, an indication that the coupling between local vibrational modes play an important role in the transport dynamics of the studied manganites.

Alternatively, to obtain order of magnitude estimates for the frequencies, we can divide (17) by (16). While nominally less accurate, this procedure is in practice more reliable for it is less sensitive to the uncertainties associated with the extraction of parameters from fits to experimental data. The division leads to an expression for the frequency $\omega^* = \sqrt{2{\omega_0}^2 - {\omega_1}^2}$ that depends only on the parameters C and D:

$$\omega^* = \sqrt{\frac{80{k_B}^2 D}{\hbar^2 C}}. \tag{25}$$

[1]For better visualization, the supporting information shows plots of $\log(\rho/T)^s$ as a function of $1/T$

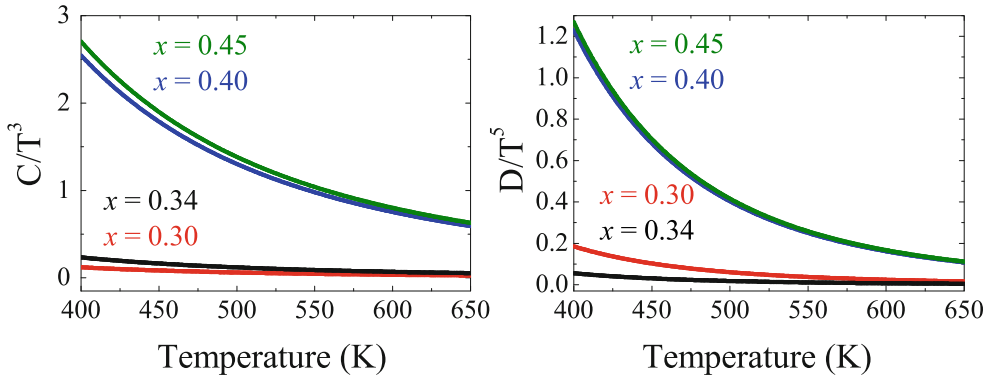

Fig. 3 (*Colored online*) Temperature dependencies of the C/T^3 and D/T^5 terms on the right-hand side of (18) for all studied samples

In the limit of decoupled local modes, $\omega_1 \to 0$, we would have $\omega^* = \sqrt{2}\omega_0$. From (21), however, we have found that $\omega_1 \approx \omega_0$, so that $\omega_0 \approx \omega^*$, and from (25), we find $\nu_0 = \omega_0/2\pi = 9.175 \times 10^{13}$ Hz and 5.039×10^{13} Hz for $x = 0.30$ and 0.45, respectively.

For comparison, Fig. 4d shows Raman spectroscopic results [25] for the frequencies ν_2 and ν_3 of the activated distortions, i. e., of the bending and stretching vibrational modes, respectively. The frequencies obtained from our analysis of the electrical resistivity—a macroscopic property—are close to the spectroscopic results, even though our estimate for the frequency ω_0 at $x = 0.45$ is substantially smaller than at $x = 0.30$, while Fig. 4d shows frequencies at $x = 0.45$ that are slightly larger than at $x = 0.30$. One cannot expect frequency estimates derived from resistivity measurements to be as accurate as spectroscopic results, and one expects the uncertainties arising in comparisons between transport properties measured at different concentration levels to be especially large, since we cannot account for the contribution of the grain boundaries in our samples, which are polycrystalline.

We have also calculated the room temperature hopping frequency Ω_0, from (19), for each concentration x. To determine the factor n in the denominator of the prefactor on the right-hand side, we relied on the equality $n = (2/V)x(1 - x)$, where V is the unit cell volume; to determine the factor a^2, we used the nearest-neighbor Mn separation as an approximation for a. The resulting Ω_0's range from 1.51×10^{14} Hz to 7.10×10^{14} Hz close to the computed ω^*'s. This order of magnitude agreement reinforces confidence in (18).

3 Conclusions

In summary, a new expression was derived for thermal dependence of the electrical resistivity for the small-polaron model in the non-adiabatic regime. In contrast with Holstein's analysis, which assumed the ratio between the energy $\hbar\omega_k$ of the vibrational modes and the thermal energy $k_B T$ to be so small that expansions to linear order of the hyperbolic functions on the right-hand side of (3) become

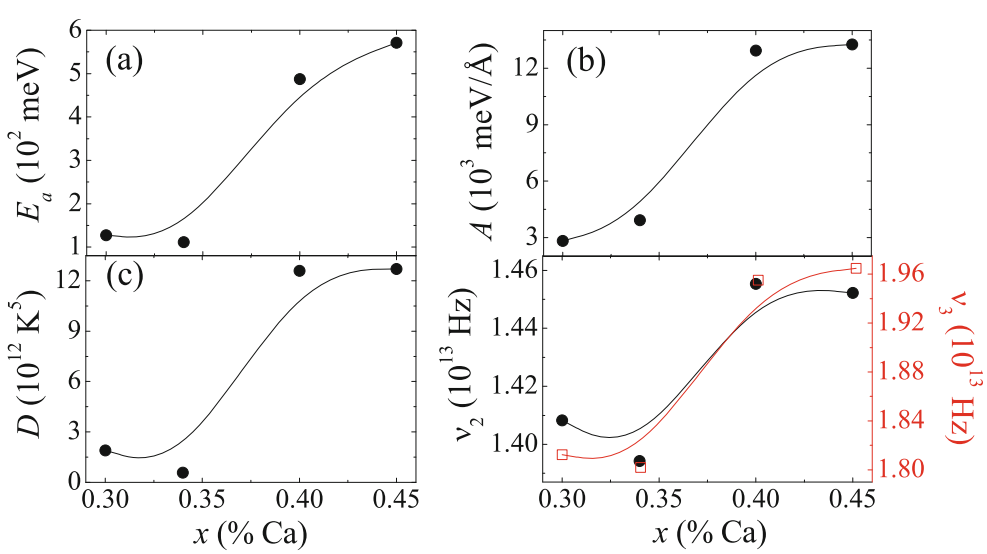

Fig. 4 (*Colored online*) Activation energy E_a, deformation coefficient A, fifth-order coefficient D, and frequencies ν_2 and ν_3 of the bending and stretching vibration modes as functions of the dopant concentration x

appropriate, our formulation includes third- and fifth-order terms in the expansion of the hyperbolic tangent in the dominant term.

Comparison with experiment showed that such higher-order terms become important at low temperatures in samples with enhanced electrical resistivities, due to higher doping. Higher activation energies E_a and polaron binding energies E_p were found for the samples with $x = 0.40$ and 0.45, an indication that the quasiparticles are more localized.

Additional study along the line of reasoning presented in this paper seems necessary, since the frequencies extracted from fitting our expression to the temperature-dependent measured resistivities only approximately match the Raman-spectroscopic results for the same samples, and since our fits involved two additional adjustable parameters, the coefficients C and D in (12). Nonetheless, the excellent agreements in the main plots of Fig. 2 suggest that at least a fraction of the deviations from (6) reported in the literature may be due to the higher-order terms neglected in Holstein's derivation of that equation. The more accurate expression for $\rho(T)$ derived in this paper should be considered before alternative physical mechanisms are proposed to explain discrepancies between the polaron model and the experimental data.

Acknowledgments This material is based upon work supported by the Brazilian agencies CNPq Grants No. 485405/2011-3 and 305772/2011-2 and FAPESP under Grants No. 2009/18618-5 and 2010/18364-0.

References

1. C. Kittel. *Introduction to solid states physics*, 8th (Berkeley, California, 2005)
2. N. W. Ashcroft, N. D. Mermin. *Solid state physics* (Orlando, Florida, 1976)
3. D. K. Ferry. *Semiconductor transport*, Taylor and Francis,1st ed. (London, 2000)
4. B. Askerov, Electron transport phenomena in semiconductors. Singapore: World Scientific, 1st ed. (1994)
5. N. F. Mott, E. A. Davies. *Electron processes in non-crystalline materials* (Clarendon, Oxford, 1979)
6. K. Tobe, T. Kimura, Y. Okimoto, Y. Tokura. Phys. Rev. B. **64**, 184421 (2001)
7. H. L. Liu, M. A. Quijada, A. M. Zibold, Y.-D. Yoon, D. B. Tanner, G. Cao, J. E. Crow, H. Berger, G. Margaritondo, L. Forr, B. Hoan, J. T. Markert, R. J. Kelly, M. Onellion. J. Phys: Condens. Matter. **11**, 239 (1999)
8. A. S. Moskvin, Phys. Rev. B. **84**, 075116 (2011)
9. E. Dagotto, T. Hotta, A. Moreo. Phys. Rep. **344**, 1 (2001)
10. T. Holstein. Ann. Phys. **8**, 325 (1959)
11. T. Holstein. Ann. Phys. **8**, 343 (1959)
12. R. Raffaelle, H. U. Anderson, D. M. Sparlin, P. E. Parris. Phys. Rev. B. **43**, 7991 (1991)
13. M. Jaime, H. T. Hardner, M. B. Salamon, M. Rubinstein, P. Dorsey, D. Emin. Phys. Rev. Lett. **78**, 951 (1997)
14. J. H. Zhao, H. P. Kundel, X. Z. Zhou, G.wyn. Williams. J. Phys: Condens. Matter. **13**, 5785 (2001)
15. M. Jaime, M. B. Salamon, M. Rubinstein, R. E. Treece, J. S. Horwitz, D. B. Chrisey. Phys.Rev. B. **54**, 11914 (1996)
16. P. Mandal, B. Bandyopadhyay, B. Ghosh. Phys. Rev. B. **64**, 180405R (2001)
17. T. Chatterji, D. Riley, F. Fauth, P. Mandal, B. Ghosh. Phys. Rev. B. **73**, 094444 (2006)
18. S.-W. Cheong, H. Y. Hwang, ed. by Y. Tokura. *In colossal magnetoresistance oxides* (Gordeon & Breach, London, 1999)
19. G. Huo, D. Song, Q. Yang, F. Dong. Ceram. Int. **34**, 497 (2008)
20. A. Karmakar, S. Majumdar, S. Giri. Phys. Rev. B. **79**, 094406 (2009)
21. A. Neetikam, I. Das, A. K. Dhiman, A. K. Nigam, D. Yadav, Bhattacharyya, S. S. Meena. J. Appl.Phys. **112**, 123913 (2012)
22. X. J. Chen, C. L. Zhang, J. S. Gardner, J. L. Sarrao, C. C. Almasan. Phys. Rev. B. **68**, 064405 (2003)
23. Yu. Kh. Vekilov, Ya. M. Mukovskii. Solid State C. **152**, 1139 (2012)
24. M. Viret, L. Ranno, J. M. D. Coey. J. Appl. Phys. **81**, 4964 (1997)
25. F. E. N. Ramirez, F. F. Ferreira, W. A. Alves, J. F. Q. Rey, J. A. Souza. J. Magn. Magn. Mater. **324** (2012)
26. J. A. Souza, H. Terashita, E. Granado, R. F. Jardim, N. F. Jr. Oliveira, R. Muccillo. Phys.Rev. B. **78**, 054411 (2008)